Earthward plasma sheet flows during substorm phases

L. Juusola,[1,2] N. Østgaard,[1] E. Tanskanen,[1,2] N. Partamies,[2] and K. Snekvik[2]

Received 18 May 2011; revised 21 July 2011; accepted 4 August 2011; published 22 October 2011.

[1] Magnetic reconnection in the Earth's magnetotail converts open magnetic flux to closed, producing fast flows in the plasma sheet. Earthward fast flows can thus be used as a proxy for energy and momentum transfer into the closed magnetosphere during the course of a substorm. Characteristics of flows observed before substorm onset can provide information on the role of the flows in substorm onset triggering as well as the sequence of substorm-related processes. We use 15 years of data obtained by Geotail, Cluster, and THEMIS to study statistically the distribution of earthward plasma sheet flows during substorms. Substorm phases are determined from time series of the AL index and the z-component of the interplanetary magnetic field. We find that the occurrence frequency of medium-speed (100 km/s < V < 500 km/s) flows increases slightly toward the end of the substorm growth phase. At substorm onset there is a sharp increase of medium-speed flows, and during substorm recovery there is a gradual decrease of such flows. The occurrence frequency of high-speed (V > 500 km/s) flows, on the other hand, does not clearly increase during the substorm growth phase. The increase at substorm onset is more gradual than for the medium-speed flows. The occurrence frequency of high-speed flows peaks at the beginning of substorm recovery. These results indicate that any effect of the flows on substorm onset triggering would be caused by medium rather than very high speed flows.

Citation: Juusola, L., N. Østgaard, E. Tanskanen, N. Partamies, and K. Snekvik (2011), Earthward plasma sheet flows during substorm phases, *J. Geophys. Res.*, *116*, A10228, doi:10.1029/2011JA016852.

1. Introduction

[2] The auroral substorm is generally divided into three phases: growth, expansion, and recovery phase [*Akasofu*, 1964; *McPherron*, 1970]. During the growth phase, the auroral oval moves equatorward, and particularly on the nightside, east-west oriented auroral arcs drifting slowly equatorward can be observed. The beginning of the substorm expansion phase is referred to as the substorm onset. The onset is signified by an auroral breakup, during which typically the equatorwardmost of the equatorward drifting arcs intensifies and forms the so-called auroral bulge. While several brightenings can occur already during the growth phase, the onset is the intensification leading to the large-scale dynamics. During the expansion phase, the auroras expand eastward, westward, and poleward from the onset location.

[3] According to the open magnetosphere model by *Dungey* [1961], the closed geomagnetic field lines reconnect with the southward interplanetary magnetic field (IMF) on the dayside magnetopause. The resulting open field lines are dragged tailward across the polar caps by the solar wind. On the nightside they reconnect again, and the resulting closed but far stretched field lines migrate back toward the dayside magnetopause. This process is known as the magnetospheric convection. Occasionally, the dayside and nightside reconnection rates are balanced, resulting in periods of steady magnetospheric convection [e.g., *Sergeev et al.*, 1996], but more often more magnetic flux is either opened or closed [e.g., *Milan et al.*, 2007]. In the magnetosphere, the substorm consists of such periods of loading and unloading [*McPherron et al.*, 1973]. The growth phase, during which magnetic flux is opened and stored in the magnetotail, is often initiated by the southward turning of the IMF. During the expansion phase, the stored energy is released explosively, and during the recovery phase, the magnetosphere returns to its quiet state [*McPherron*, 1979]. Tail magnetic field stretching during the substorm growth phase is associated with an intensification and thinning of the tail current sheet, while the magnetic field dipolarization during the substorm expansion phase is connected to a disruption of the tail current. During the substorm recovery phase the tail returns to its ground state with a moderately stretched magnetic field [*McPherron et al.*, 1973].

[4] Tail reconnection is the process that converts open magnetic flux to closed. The related conversion of magnetic to kinetic energy produces fast flows in the plasma sheet. Thus fast flows can be used as a proxy for the energy and momentum transfer into the closed magnetosphere [*Baumjohann et al.*, 1989; *Angelopoulos et al.*, 1994].

[5] The average ion flow speed in the central plasma sheet is low, below 100 km/s, due to the predominance of low-speed flows. High-speed flows occur in bursts mostly less than 10 s in duration, with intermittent intervals of near

[1]Department of Physics and Technology, University of Bergen, Bergen, Norway.
[2]Finnish Meteorological Institute, Helsinki, Finland.

0148-0227/11/2011JA016852

stagnant plasma [*Baumjohann et al.*, 1989, 1990]. The bursts organize themselves in 10-min timescale flow enhancements, termed bursty bulk flow (BBF) events [*Angelopoulos et al.*, 1992]. An often used threshold for high-speed flows is $V > 400$ km/s [*Baumjohann et al.*, 1990; *Angelopoulos et al.*, 1992; *Shiokawa et al.*, 1997], and BBFs are defined as segments of $V > 100$ km/s in the plasma sheet, during which V exceeded 400 km/s for at least at one sample [*Angelopoulos et al.*, 1993, 1994].

[6] High-speed flows are almost always directed earthward between $-19\ R_E < x_{GSM} < -9\ R_E$ (Earth radii), indicating that their source is beyond $x_{GSM} < -19\ R_E$ [*Shiokawa et al.*, 1997]. Earthward of $x_{GSM} = -19\ R_E$, the occurrence rate of BBFs decreases. Braking of the flow speed has been suggested as a possible explanation [*Angelopoulos et al.*, 1994]. The largest occurrence rates of high-speed flows are found near the midnight meridian [*Baumjohann et al.*, 1990]. The flow peaks are usually associated with magnetic field dipolarization [*Angelopoulos et al.*, 1992]. The bursts are more frequent during geomagnetically disturbed times but occur also during low auroral electrojet (AE) index conditions [*Baumjohann et al.*, 1989; *Angelopoulos et al.*, 1994]. Although BBFs occur only 10–15% of the time, they have been estimated to be responsible for 60–100% of the earthward transport of mass, energy, and magnetic flux [*Angelopoulos et al.*, 1994].

[7] Mainly two kinds of auroral signatures have been observed during BBFs: small expansions and auroral streamers [*Nakamura et al.*, 2001a, 2001b]. Streamers occur when the auroral oval is wide, both during substorm and nonsubstorm times. They originate at the activated poleward boundary (poleward boundary intensification, PBI) of the auroral oval and propagate toward the equatorward boundary. Several streamers frequently evolve simultaneously [e.g., *Amm and Kauristie*, 2002]. Dynamic intensifications of substorm activity during the expansion and early recovery phases involve formations of streamers [*Henderson et al.*, 1998].

[8] One of the key open questions about substorms concerns the formation of the substorm current wedge [*McPherron et al.*, 1973]. According to the near-Earth neutral line model [*Baker et al.*, 1996], a thin tail current sheet becomes unstable, possibly due to the tearing mode instability, leading to the formation of a reconnection region at about 20–30 R_E distance from Earth. Because the reconnection rate is proportional to the Alfvén speed of the inflowing plasma, the process is relatively slow as long as it remains on the closed magnetic field lines where plasma is abundant. After the last closed field line is reached, the reconnection rate increases abruptly, which is often interpreted as the onset of the expansion phase. Dipolarization and fast plasma sheet flows are caused by the outflow from the reconnection region, and the substorm current wedge forms as the newly reconnected flux tubes deposit their magnetic flux at the inner edge of the plasma sheet.

[9] According to the current disruption model [e.g., *Lui et al.*, 2008], on the other hand, local instabilities lead to current disruption within about 15 R_E from Earth. The current disruption causes the magnetic field to relax to a more dipolar configuration, which gives rise to dipolarization and fast flows. The current disruption process instigates further disruption in the adjacent regions by thinning the plasma sheet and enhancing the cross-tail current, which allows the current disruption to occur progressively down the magnetotail. Later, magnetic reconnection may develop at one of these current disruption sites.

[10] Recently, *Nishimura et al.* [2010a, 2010b] used THEMIS all-sky imager data to show that there is a distinct and repeatable sequence of events leading to a substorm auroral onset: a PBI followed by a north-south arc moving equatorward toward the onset latitude. Because of the linkage of fast magnetotail flows to PBIs and north-south auroras, the results indicate that an onset is preceded by enhanced earthward plasma flows associated with enhanced reconnection near the preexisting open-closed field line boundary.

[11] However, the detection of a fast earthward flow in the plasma sheet does not always lead to substorm activity. *Ohtani et al.* [2006] studied the response of the geosynchronous magnetic field to earthward plasma sheet flows. Dipolarization at the geosynchronous orbit could be regarded as a manifestation of tail current disruption. They found that in most events the fast flows ($V_{\perp,x} > 300$ km/s) do not reach geosynchronous orbit and that the generation of a fast flows is not enough to cause dipolarization at the orbit.

[12] Plasma sheet flows are thus highly relevant to substorms. Moreover, characteristics of any flows observed before the substorm onset can provide information on the role of the flows in substorm onset triggering. In this study we examine statistically, how the earthward plasma sheet flows of different speeds at radial distance <30 R_E are distributed between the substorm phases. We begin with an introduction of the used instruments and data analysis techniques (section 2). In section 3, a method for automatic recognition of substorm phases from time series of the AL index and IMF B_z is described. In section 4, the earthward plasma sheet samples from the Cluster, Geotail, and THEMIS satellites are categorized according to speed into 10 bins (0–100 km/s, 100–200 km/s, …, 900–1000 km/s), and the distribution of the flows between different substorm phases is examined. Sections 5 and 6 contain discussion and conclusions.

2. Data

[13] In this study we have used magnetospheric ion and magnetic field data obtained by the Cluster 1 and 3 satellites from 2001 to 2007, by the Geotail satellite from 1995 to 2006, and by the THEMIS 1–5 satellites from September 2007 to the end of 2009. From the Cluster 1 and 3 spacecraft we have used 4-s (spin average) resolution data from the Fluxgate Magnetometer (FGM) [*Balogh et al.*, 2001] and ion moments from Cluster Ion Spectrometry (CIS) [*Rème et al.*, 2001] Hot Ion Analyser (HIA) instrument. CIS HIA measures energies from 5 eV/q to 32 keV/q. From the Geotail spacecraft we have utilized 3-s (spin average) resolution data from the Magnetic Field experiment (MGF) [*Kokubun et al.*, 1994], and 12-s resolution ion moments from the Low Energy Particle experiment (LEP) [*Mukai et al.*, 1994]. LEP Energy-per-charge Analyzer (EA) measures energies from several eV/q to 43 keV/q. From the THEMIS 1–5 spacecraft we have used 3-s (spin average) resolution data from the Fluxgate Magnetometer (FGM) [*Auster et al.*, 2008], and ion moments from the Electrostatic Analyzer (ESA) [*McFadden et al.*,

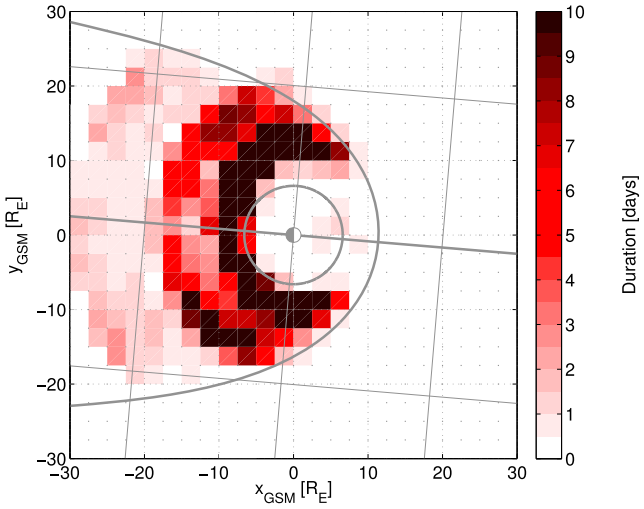

Figure 1. Combined observation time by Cluster 1 and 3 from 2001 to 2007, by Geotail from 1995 to 2006, and by THEMIS 1–5 from September 2007 to the end of 2009 of earthward ($V_x \geq 0$) plasma sheet ($\beta > 0.5$) flows on a 2.5 R_E × 2.5 R_E grid, presented as a function of GSM x and y. The gray circle indicates the geostationary orbit at 6.6 R_E radial distance, and the gray curve the magnetopause according to *Shue et al.* [1997], with P_{dyn} = 1 nPa and IMF B_z = 0. Both the magnetopause and the solid grid have been rotated 4.8° clockwise to take into account the aberration due to Earth's orbital motion. The thick line shows the aberrated noon-midnight axis.

2008a, 2008b]. ESA measures energies from 1.6 eV/q to 25 keV/q.

[14] We have investigated how earthward ($V_x \geq 0$) plasma sheet ($\beta > 0.5$ [*Angelopoulos et al.*, 1993, 1994]) flows with speeds $0 \leq V < 1000$ km/s are distributed between substorm phases. Figure 1 displays the total duration of observations (color) of these flows on a 2.5 R_E × 2.5 R_E grid, presented as a function of x and y. We have used Cartesian (x, y, z) Geocentric Solar Magnetospheric (GSM) coordinates. The gray circle represents the geostationary orbit at 6.6 R_E radial distance, and the gray curve the magnetopause according to *Shue et al.* [1997], with P_{dyn} = 1 nPa and IMF B_z = 0. Both the magnetopause and the solid grid have been rotated 4.8° clockwise to take into account the aberration due to Earth's orbital motion. The thick line shows the aberrated noon-midnight axis. In the equatorial plane, the observations covered distances up to about 30 R_E from Earth.

[15] Because of the large amount of data, we began by dividing our samples into "flow events," represented by averages of the ion and magnetic field measurements during the event. Since plasma sheet convection is dominated by slow speed flows, a flow event was defined as a continuous block of samples, during which $\beta > 0.5$ and the flow speed remained within one of the bins: 0–100 km/s, 100–200 km/s, …, 900–1000 km/s. Flow events consisting of one data point only were not included. Typical duration of the events varied from seconds to minutes.

[16] In section 4.1, the speed distribution of plasma sheet flows during substorm phases will be investigated. Only information about the begin and end times as well as the characteristic speed range of each flow event were needed for that analysis. In section 4.2, spatial distribution of plasma sheet magnetic field and speed during substorm phases will be presented. The production of such maps required some further processing of the data: In order to emphasize the bulk flows in the center of the plasma sheet, the ion moment and magnetic field averages were weighted by β

$$\bar{x} = \frac{\sum_{i=1}^{n} \beta_i x_i}{\sum_{i=1}^{n} \beta_i}. \quad (1)$$

These event means were then gridded according to their xy locations, and averages of the event averages, weighted by the durations of the events, were computed for each grid point.

[17] For determining the substorm phase during each flow event, solar wind data at 1-min resolution propagated to Earth's bow shock nose were extracted from NASA/GSFC's OMNI data set through the OMNIWeb interface (http://omniweb.gsfc.nasa.gov/). The auroral electrojet indices (AE, AL, AU) at 1-min resolution were obtained from the World Data Center for Geomagnetism, Kyoto (http://wdc.kugi.kyoto-u.ac.jp/index.html).

3. Determination of Substorm Phases

[18] It is clear that visual identification of substorms is very subjective. *Frey* [2010] already noted that the scientific community should attempt to establish generally accepted criteria for identifying substorm onsets and advance from the qualitative approach to a more quantitative one. Our approach is an attempt to move in that direction.

[19] In addition to optical signatures, substorm phases can also be recognized from ground-based magnetometer observations, such as the Auroral Electrojet (AE) [*Davis and Sugiura*, 1966] index. The limited coverage of the AE stations may lead to some ambiguity in the exact timing of substorm phases and amplitudes and for small localized disturbances or disturbances occurring significantly poleward or equatorward of the AE stations to be missed altogether. We chose to use AE because it provides nearly continuous data from 1995 to 2009, which is essential for our analysis.

[20] Figure 2 illustrates the general behavior of AE, as well as the westward (AL) and eastward (AU) auroral electrojet indices during the course of a substorm. Displayed are the superposed epoch medians of the AE, AL, and AU indices as well as the interplanetary magnetic field (IMF) z-component (B_z) as a function of time. The 4193 substorm onset times between May 2000 and December 2005 as determined by *Frey et al.* [2004]; *Frey and Mende* [2006] based on IMAGE satellite data were used as zero epochs. The accuracy of the IMAGE onset time determination is 2 min. The error bars (shaded area) show the 15.9 and 84.1 percentiles of AL. For a normal or Gaussian distribution, 68.3% of the values lie within one standard deviation from the mean, and hence 2 × 15.9% of the values lie outside. The vertical black lines mark the approximate substorm phases, as determined from the AL curve: the growth phase, marked by the slow decrease in AL, started to show up about 1 h 15 min before the auroral onset, although IMF B_z turned southward already

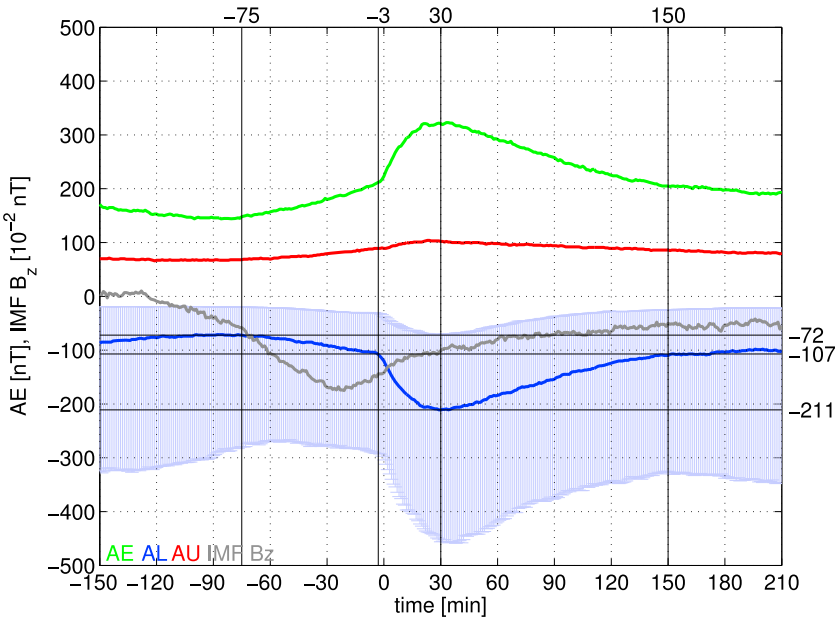

Figure 2. Superposed epoch medians of the AE, AL, and AU indices and the IMF B_z as a function of time. The 4193 substorm onset times between May 2000 and December 2005 as determined by *Frey et al.* [2004] and *Frey and Mende* [2006] based on IMAGE satellite data were used as zero epochs. The accuracy of the IMAGE onset time determination is 2 min. The error bars show the 15.9 and 84.1 percentiles of AL. The four vertical black lines mark the approximate substorm phases, as determined from the AL curve: the beginning of the growth phase around −75 min, the beginning of the expansion phase around −3 min, the beginning of the recovery phase around +30 min, and the end of the recovery phase around +150 min. The numbers on the right-hand side are the median AL values corresponding to times marked by the vertical black lines.

45 min earlier. The AL onset, marked by the beginning of the sharp decrease, occurred 3 min before the auroral onset. The expansion phase ended and recovery phase began 30 min after the auroral onset, when AL started to increase again. The recovery phase ended 2 h after the expansion, when AL had approximately returned to its preonset level. Altogether, from the southward turning of IMF B_z to the end of the recovery phase, the substorm lasted about 4 h 30 min.

[21] On average, substorms occur at a rate of about four per day [*Borovsky et al.*, 1993], although during intense solar wind driving they take place more frequently and are more intense, while during weak solar wind driving, long quiet periods can occur. One problem with an automatic determination of substorm phases is that individual substorms often differ considerably from each other. Particularly during storm periods, the expansion phase of a new substorm may begin before the recovery phase of the previous one has ended. The duration of the different phases varies considerably, and the end of the recovery phase is not always unambiguous. It is also common for several activations to occur during one substorm. During the growth phase, smaller activations that do not lead to the global reconfiguration of the tail magnetic field may take place. These activations, called pseudobreakups, are localized and only last for a few up to about ten of minutes [e.g., *Koskinen et al.*, 1993].

[22] The median value for AL during the included 15 year period was −50 nT, and the median for negative values of the time derivative of AL (dAL/dt) was −4 nT/min. These median values were used as a basis for separating quiet periods from active ones. The quiet periods were assumed to comprise nonsubstorm intervals and substorm growth phases, and the active periods comprised substorm expansion and recovery phases.

[23] To identify the substorm phases, we used the following criteria. For expansion, the criteria are a rapid decrease in AL (dAL/dt < −4 nT/min) and AL decreases below −50 nT. For recovery, the criterion is AL < −50 nT and for growth, the criterion is IMF B_z < 0.

[24] The above conditions generally resulted in intervals that lasted a few minutes. In order to produce substorm phases that matched the large-scale behavior of AL, intervals meeting the same conditions within 50 nT/4 nT/min = 12.5 min of each other were grouped together, regardless of any samples in between that did not meet these conditions. This "characteristic substorm phase time" would correspond to the expansion phase duration of the weakest acceptable substorm, assuming that before the onset AL was zero. The resulting substorm expansion phases were trimmed such that they began at the local AL maximum inside the expansion phase interval and ended at the AL minimum. Phases including only one data point were discarded.

[25] The definitions and grouping produced partially overlapping substorm phases. As at any moment of time there could only be one phase, the different phases were given a priority, (1) substorm expansion phase, (2) substorm recovery phase, (3) substorm growth phase, and the phase with a higher priority was retained. Naturally, IMF can be

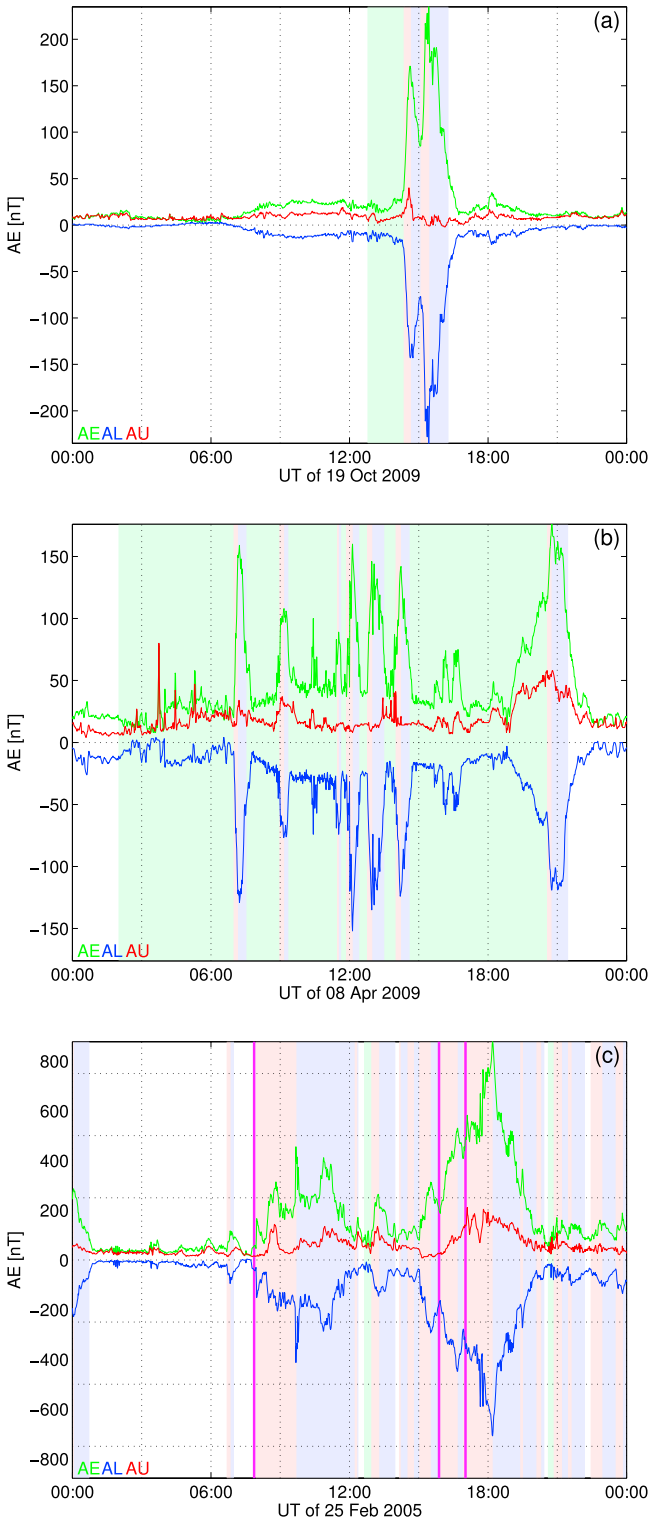

Figure 3. Time series of the AE, AL, and AU indices on (a) 19 October 2009, (b) 08 April 2009, and (c) 25 February 2005. The green, red, and blue shadings mark the substorm growth, expansion, and recovery phases as given by the method described in section 3. The vertical magenta lines in Figure 3c mark substorm onsets observed by the IMAGE satellite.

southward also during substorm expansion and recovery phases, which is why the growth phase was given the lowest priority. A new substorm expansion phase sometimes begins before the recovery phase of the previous one has ended. In order to avoid categorizing such expansion phases as part of the recovery phase of the previous substorm, the expansion phase was given a higher priority than the recovery phase. Moreover, a growth phase was expected to precede and a recovery phase to follow an expansion phase. Finally, periods not belonging to any of the four categories were labeled as nonsubstorm intervals.

[26] Examples of the resulting categorization are given in Figure 3, which displays a time series of the AE, AL, and AU indices for three different days. The substorm growth, expansion, and recovery phases are marked by green, red, and blue shading, respectively. Figure 3a shows a relatively simple event with a growth phase followed by two successive substorms consisting of an expansion phase and a recovery phase. Figure 3b shows a more complicated event with several substorms occurring during a prolonged period of negative IMF B_z. Figure 3c shows an active event typical for storm periods. The major AL decrease consisted of several successive substorms. For comparison, the vertical magenta lines in Figure 3c mark substorm onsets as observed by the IMAGE satellite. All three lines coincide very well with the AL substorm onsets marked by the beginning of the red shading.

[27] The substorm phase recognition method resulted in a growth phase during 10% of the time, expansion phase in 16%, and recovery phase in 33%. During active periods, such as that shown in Figure 3c, growth phases were often displaced by the higher priority expansion and recovery phases, resulting in the relatively small growth phase percentage. Using Polar UVI images, *Kullen and Karlsson* [2004] found that substorms are present during 50% of observation time. As it is not possible to determine the start of the growth phase from Polar UVI images, their substorms included only expansion and recovery phases. Our corresponding percentage, 49%, is in good agreement with theirs.

[28] According to our method, the median duration for the growth phase was 31 min (15.9-percentile: 12 min, 84.1-percentile: 1 h 25 min, average: 48 min), for the expansion phase 12 min (3 min, 44 min, 24 min), and for the recovery phase 31 min (14 min, 1 h 20 min, 48 min). *Tanskanen* [2009] developed a similar automated search engine for IMAGE magnetometer network data. They found that the average substorm duration from the beginning of the growth phase to the end of the recovery phase for the years 1993–2003 was 3 h 5 min. According to *Kullen and Karlsson* [2004], the average lifetime of the combined expansion and recovery phases is 1.3 h for small and medium sized auroral oval conditions and 2.3 h for large auroral oval conditions. *Jayachandran and MacDougall* [2007] studied 26 substorms and found that the average growth, expansion, and recovery phase times determined from polar cap convection measurements are 31.6, 22.4, and 38.8 min, respectively, whereas the average growth and expansion phase times determined from the geosynchronous magnetic field measurements are 51.2 and 5.8 min. Using images from the Earth Camera on Polar, *Hoffman et al.* [2010] reported that the substorm expansion phase is much shorter for storm main phase (15 min) than for isolated substorms (30 min).

Using the hemispheric power computed from Polar UVI observations, *Chua et al.* [2004] found that the mean and median substorm expansion times are 26 and 18 min during northward IMF conditions, and 36 and 33 min during southward IMF conditions, respectively. There is some variation between these durations depending on the type of data used, but ours are of the same order of magnitude.

4. Results

[29] In this section we investigate how earthward plasma sheet flows of different speeds are distributed between the substorm phases. Of the time the spacecraft spent in the plasma sheet ($\beta > 0.5$) observing earthward ($V_x \geq 0$) flows (Figure 1), 56% took place during nonsubstorm, 12% during substorm growth phase, 11% during substorm expansion phase, and 21% during substorm recovery phase conditions.

4.1. Speed Distribution of Plasma Sheet Flows During Substorm Phases

[30] Figure 4a displays the percentage of each substorm phase time during the observation of earthward plasma sheet flows with speeds $0 \leq V < 100$ km/s ($V = \sqrt{V_x^2 + V_y^2 + V_z^2}$) relative to the same substorm phase time during the observation of earthward plasma sheet flows with speeds $0 \leq V <$ 1000 km/s. Figures 4b–4j show the same for the speed bins 100 km/s $\leq V <$ 200 km/s, 200 km/s $\leq V <$ 300 km/s, 300 km/s $\leq V <$ 400 km/s, 400 km/s $\leq V <$ 500 km/s, 500 km/s $\leq V <$ 600 km/s, 600 km/s $\leq V <$ 700 km/s, 700 km/s $\leq V <$ 800 km/s, 800 km/s $\leq V <$ 900 km/s, and 900 km/s $\leq V <$ 1000 km/s. In order to determine the temporal development of the distributions, the substorm growth, expansion, and recovery phases have been further divided into five bins by normalizing the duration of each phase to 1. The sum of all None-bars in Figures 4a–4j, for instance, is 100%. Thus the relative heights of the bars in one panel represent the relative occurrence frequencies of the flows.

[31] The majority of all earthward plasma sheet flow observations during all substorm phases consisted of slow speed ($V <$ 100 km/s) flows, although the percentage was somewhat higher for nonsubstorm (97%) and substorm growth phases (96%) than for substorm expansion (89%) or recovery phases (90%). The distributions for the higher speed ($V \geq$ 100 km/s) flows were clearly different from that of the slow flows, but shared common features among themselves: generally, the frequency of the flows was smallest during nonsubstorm conditions. The higher the speed was, the less likely it was for such flows to be observed outside substorms. The frequency was only slightly higher during the substorm growth phase than during nonsubstorm periods, and had a tendency to increase toward the end of the growth phase. This is particularly obvious for the 100 km/s $\leq V <$ 200 km/s and 200 km/s $\leq V <$ 300 km/s bins. At the substorm onset, that is, at the beginning of the substorm expansion phase, the frequency increased sharply, and remained elevated throughout the substorm expansion and recovery phases. The maximum occurred at the end of the expansion phase or at the beginning of the recovery phase. Toward the end of the recovery phase, the frequency decreased.

4.2. Spatial Distribution of Plasma Sheet Magnetic Field and Speed During Substorm Phases

[32] Figures 5a, 5c, and 5e show maps of the mean magnetic field z-component (B_z) in the plasma sheet during the substorm growth, expansion, and recovery phase, respectively. A background map of mean B_z during nonsubstorm conditions has been subtracted. The reason for subtracting the background was to make the relatively weak differences easier to discern. During the substorm growth phase, B_z was in general smaller than during nonsubstorm periods, except around the midnight axis, where ΔB_z was near zero. During the substorm expansion and recovery phases, ΔB_z was also negative at the edges of the plasma sheet, but around the midnight axis, there was a clear channel of positive ΔB_z. This channel was somewhat stronger and wider during the recovery phase than during the expansion phase.

[33] Figures 5b, 5d, and 5f display maps of the mean ion speed (V) in the plasma sheet during substorm growth, expansion, and recovery phases, respectively. A background map of mean V during nonsubstorm conditions has been subtracted. During all substorm phases, the speed was higher than during nonsubstorm conditions, although the effect was much stronger during the substorm expansion and recovery phases than during the substorm growth phase.

5. Discussion

[34] The white part in Figure 4a shows in reverse the combined behavior of all $V >$ 100 km/s flows. The gradual increase in the occurrence frequency of higher-speed flows toward the end of the growth phase is clearly visible. The substorm onset is like a dam breaking: suddenly, the trickle becomes a flood as energy flows into the closed magnetosphere from the unloading lobes. The higher level is maintained relatively constant throughout the substorm expansion phase and the early recovery phase. During the later recovery phase the occurrence frequency of the flows decreases. This is in agreement with the observation that auroral streamers form at the dynamic intensifications of substorm activity during the expansion and early recovery phases [*Henderson et al.*, 1998].

[35] The varying axes in Figure 4 illustrate how the observation times of the flows decrease markedly with increasing flow speed. Thus the above picture is dominated by the behavior of medium speed flows between approximately 100 km/s and 500 km/s. The more rare high-speed flows above 500 km/s do not display such a clear increase of occurrence frequency during the substorm growth phase. Neither is the increase at the substorm onset so dramatic, but the occurrence frequency increases more gradually toward a clear peak at the beginning of the recovery phase. Thus although substorm onset is preceded by flows with increased speed, the speeds are still not very high. The highest-speed flows are mainly observed rather late during the course of the substorm, at the beginning of the recovery phase. These results agree with those of *Nishimura et al.* [2010a, 2010b]. Moreover, if the flows do play a role in substorm onset triggering, our results indicate that such flows would be of medium rather than very high speed. Of course, it is possible that any high-speed flows connected to substorm onset are simply so localized that they do not appear in our statistics.

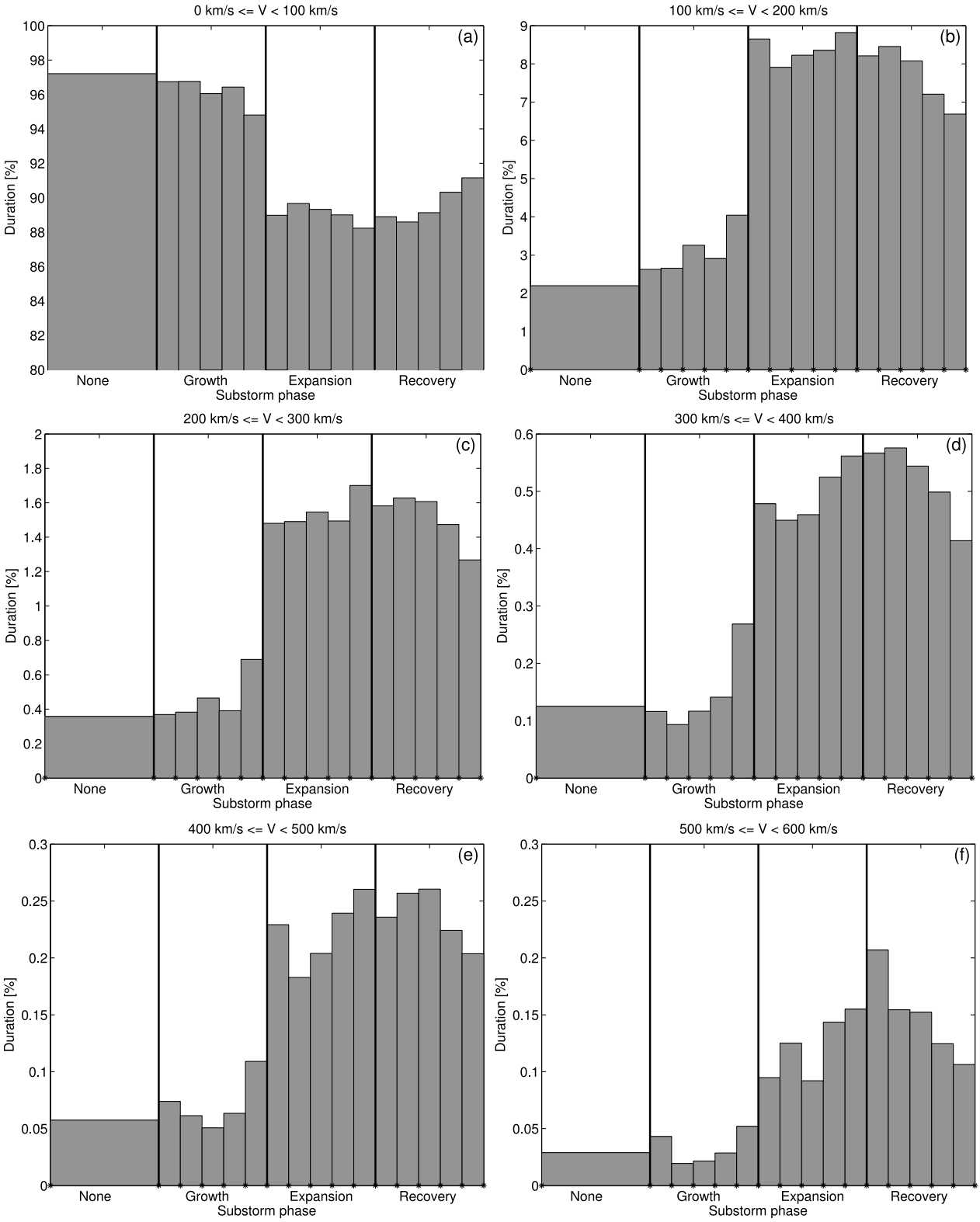

Figure 4. Percentage of each substorm phase time during the observation of earthward plasma sheet flows with speeds ($V = \sqrt{V_x^2 + V_y^2 + V_z^2}$) (a) $0 \le V < 100$ km/s, (b) 100 km/s $\le V < 200$ km/s, (c) 200 km/s $\le V < 300$ km/s, (d) 300 km/s $\le V < 400$ km/s, (e) 400 km/s $\le V < 500$ km/s, (f) 500 km/s $\le V < 600$ km/s, (g) 600 km/s $\le V < 700$ km/s, (h) 700 km/s $\le V < 800$ km/s, (i) 800 km/s $\le V < 900$ km/s, and (j) 900 km/s $\le V < 1000$ km/s relative to the same substorm phase time during the observation of earthward plasma sheet flows with speeds $0 \le V < 1000$ km/s. The substorm growth, expansion, and recovery phases have been further divided into five parts by normalizing the duration of each phase to 1.

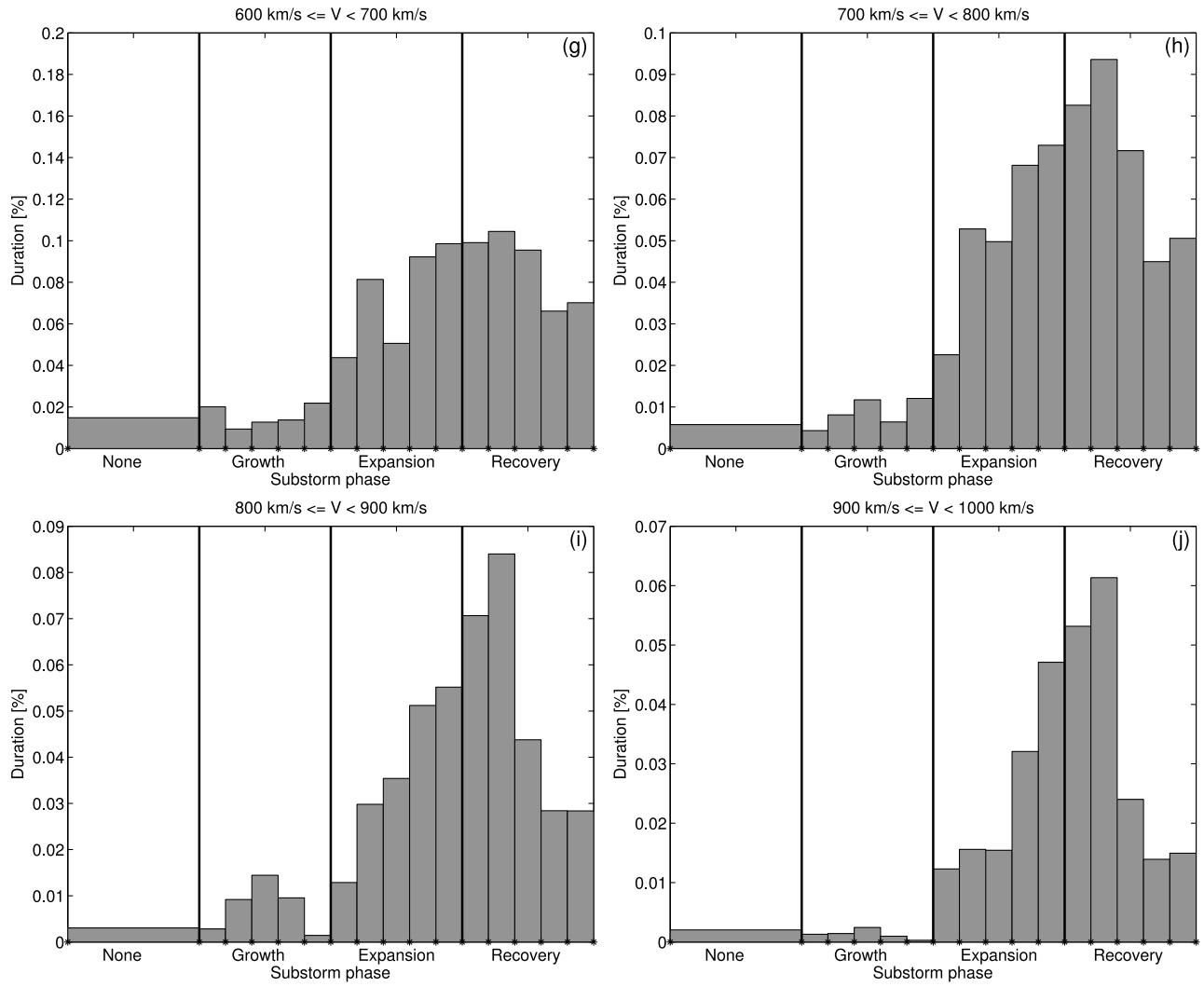

Figure 4. (continued)

Ohtani et al. [2006] have also shown that a fast ($V_{\perp,x}$ > 300 km/s) earthward flow in the plasma sheet does not always lead to substorm activity.

[36] In addition to the occurrence frequency of flows during substorms, the approximate speed limit of 500 km/s is also related to the characteristics of the flows themselves. *Juusola et al.* [2011] studied statistically the characteristics of plasma sheet flows of different speeds. They reported that plasma sheet convection is dominated by slow speed (<100 km/s) flows that circulate around Earth on both sides toward the dayside, but with increasing flow speed the sunward component of the flow velocity becomes more pronounced such that flows with V > 500 km/s are directed almost purely sunward.

[37] As we have used the AL index and an automated search engine to find the substorm phases, there is bound to be some ambiguity in the timing. For instance, in case of a double peaked substorm with the first peak stronger than the last one, such as the last substorm in Figure 3b, the time of the first peak was picked for the end of the substorm expansion phase. Moreover, it is possible that the small intensifications between 15 and 18 UT, that according to the present categorization might be called pseudobreakups, were actually weak substorms. Thus it is likely that some flows have an uncertain substorm phase label. The slightly increased occurrence frequency of higher-speed flows at the early (Figures 4e–4g) or middle part of the growth phase (Figure 4i), for instance, might be related to the pseudobreakups. However, the clear changes in the occurrence frequencies at the substorm onset and at the beginning of the substorm recovery phase indicate that the majority of the flows should be correctly labeled. The slow increase in the frequency of the higher-speed flows during the growth phase, the sharp increase at the substorm onset, the maximum occurring at the end of the expansion phase, and the decrease during the recovery phase coincide well with the typical behavior of the AL index. Thus AL appears to be a surprisingly good proxy for nightside reconnection efficiency. Furthermore, it might be possible to use the plasma sheet flow behavior to recognize the ongoing substorm phase.

[38] During the substorm growth, expansion, and recovery phases, B_z was in general smaller than during nonsubstorm times at the dawn and dusk flanks of the plasma sheet. This

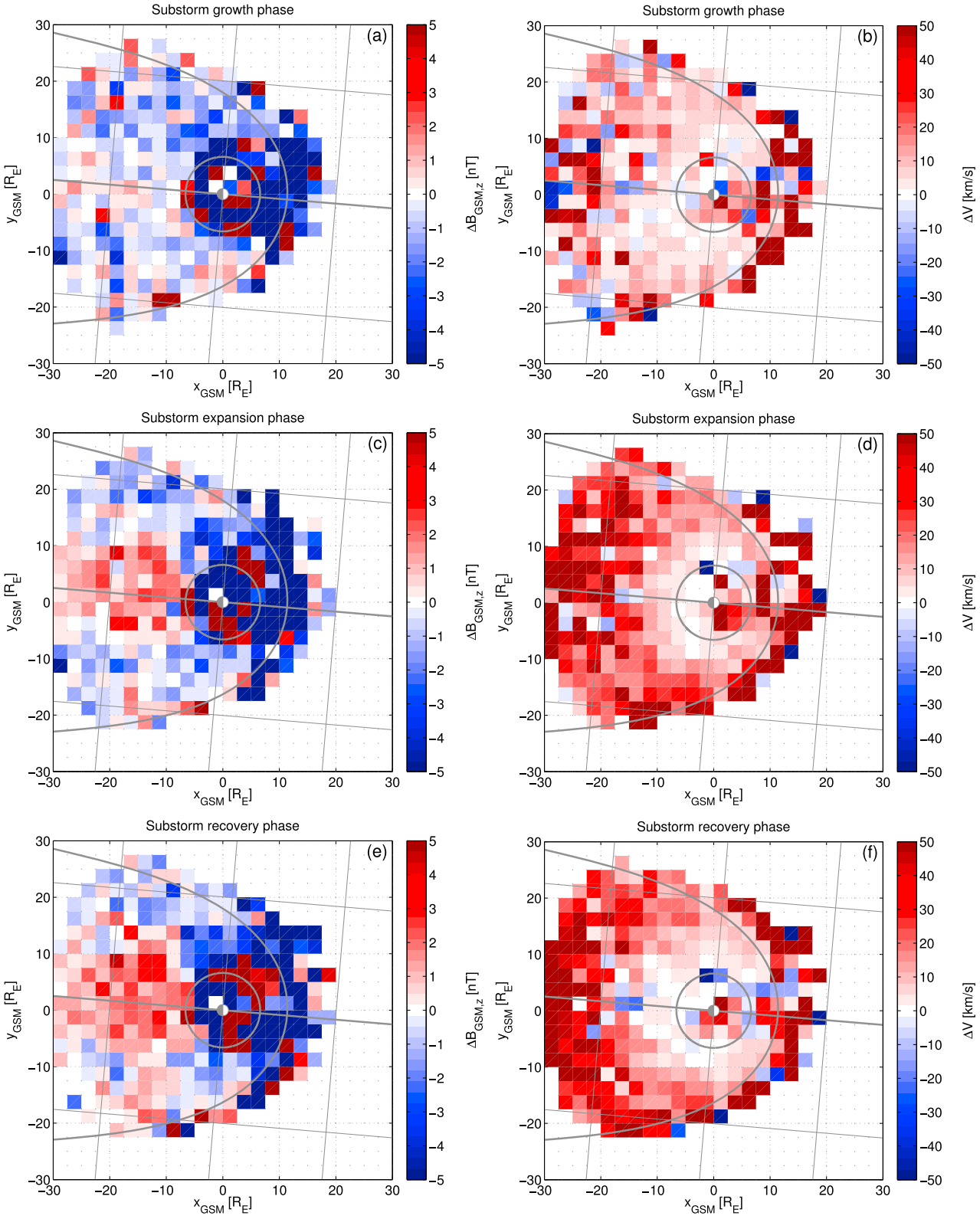

Figure 5. (a) Magnetic field z-component (B_z) for all $\beta > 0.5$, $V_x \geq 0$, and $0 \leq V < 1000$ km/s samples observed by Cluster, Geotail, and THEMIS during substorm growth phase conditions with a background of mean B_z during nonsubstorm conditions subtracted. (b) Mean ion speed (V) during substorm growth phase conditions minus background. (c) B_z during substorm expansion phase conditions minus background. (d) V during substorm expansion phase conditions minus background. (e) B_z during substorm recovery phase conditions minus background. (f) V during substorm recovery phase conditions minus background.

was most likely caused by penetration of the ambient southward IMF and tail magnetic field stretching. Furthermore, during the substorm expansion and recovery phases, a channel of increased B_z was formed around the midnight axis, probably as a result of dipolarization and flux pileup related to the earthward flows [*Angelopoulos et al.*, 1992]. The appearance of the dipolarization channel during the substorm expansion phase is in agreement with the results of *Miyashita et al.* [2009].

[39] During the substorm expansion and recovery phases, the mean convection speed in the plasma sheet was in general higher than during nonsubstorm times. During the substorm recovery phase, this enhancement was rather symmetrically distributed around the aberrated midnight axis, but during the substorm expansion phase, the average speed was more enhanced on the duskside than dawnside. Moreover, during the substorm recovery phase, the mean convection speed was decreased around the midnight axis between about $-18\ R_E < x < -10\ R_E$, indicating that the flows could not penetrate into the region of highly dipolarized field. During the substorm growth phase, the mean speed was slightly increased. The strongest increase of the earthward speed during both the substorm expansion and recovery phase was observed at the tailwardmost limit of our observations at $x = -30\ R_E$, indicating that, on average, the X-line had to be located tailward of this point. Also the dipolarization channel extended at least down to this point.

6. Conclusions

[40] In this study, 15 years of data obtained by Cluster, Geotail, and THEMIS have been used to examine statistically how earthward plasma sheet flows of different speeds are distributed between the substorm phases. The substorm phases were determined from a time series of the AL index and IMF B_z using an automated method developed for the purpose. All flow events were categorized as belonging either into a nonsubstorm, substorm growth phase, substorm expansion phase, or substorm recovery phase period. There appeared to be two distinct classes of earthward plasma sheet flows: the occurrence frequency of the vastly dominant slow speed (<100 km/s) flows decreases during substorms, while the occurrence frequency of higher speed flows increases. Our main results are as follows:

6.1. Substorm Growth Phase

[41] The occurrence frequency of medium-speed ($100\ km/s < V < 500\ km/s$) flows increases slightly toward the end of the substorm growth phase, but not that of the high-speed ($V > 500$ km/s) flows. This indicates that any effect of the flows in substorm onset triggering would be caused by medium rather than very high speed flows. ΔB_z is negative at the outer reaches of the plasma sheet, most likely because of the penetration of the ambient southward IMF.

6.2. Substorm Expansion Phase

[42] The occurrence frequency of medium-speed flows increases sharply at the beginning of the substorm expansion phase and the increased level is maintained throughout the entire phase. The occurrence frequency of high-speed flows increases more gradually toward a peak at the beginning of the recovery phase. ΔB_z is negative at the outer reaches of the plasma sheet. ΔB_z is positive around the midnight axis, most likely as a result of dipolarization and flux pileup.

6.3. Substorm Recovery Phase

[43] The occurrence frequency of all higher-speed flows decreases toward the end of the substorm recovery phase. ΔB_z is negative at the outer reaches of the plasma sheet and positive around the midnight axis. The positive ΔB_z is probably related to the high occurrence frequency of high-speed flows particularly at the beginning of the substorm recovery phase.

[44] **Acknowledgments.** We acknowledge the principal investigators E. Lucek (Cluster/FGM), I. Dandouras (Cluster/CIS), T. Nagai (Geotail/MGF), and Y. Saito (Geotail/LEP). We acknowledge NASA contract NAS5-02099 and V. Angelopoulos for use of data from the THEMIS Mission. Specifically, we acknowledge C. W. Carlson and J. P. McFadden for use of ESA data and K. H. Glassmeier, U. Auster, and W. Baumjohann for the use of FGM data provided under the lead of the Technical University of Braunschweig and with financial support through the German Ministry for Economy and Technology and the German Center for Aviation and Space (DLR) under contract 50 OC 0302. Cluster data were acquired through Cluster Active Archive, and Geotail (Editor-A) and THEMIS data were acquired through CDAWeb. We acknowledge NASA/GSFC's Space Physics Data Facility's OMNIWeb service and OMNI data. The work of L. Juusola was supported by the Norwegian Research Council, through the Norwegian Cluster project 197639/V30 and by the Academy of Finland project 137900. The work of E. Tanskanen was supported by the Academy of Finland projects 108518 and 128189.

[45] Masaki Fujimoto thanks the reviewers for their assistance in evaluating this manuscript.

References

Akasofu, S.-I. (1964), The development of the auroral substorm, *Planet. Space Sci.*, *12*, 273–282.

Amm, O., and K. Kauristie (2002), Ionospheric signatures of bursty bulk flows, *Surv. Geophys.*, *23*, 1–32.

Angelopoulos, V., W. Baumjohann, C. Kennel, F. Coroniti, M. Kivelson, R. Pellat, R. Walker, H. Lühr, and G. Paschmann (1992), Bursty bulk flows in the inner central plasma sheet, *J. Geophys. Res.*, *97*, 4027–4039.

Angelopoulos, V., et al. (1993), Characteristics of ion flow in the quiet state of the inner plasma sheet, *Geophys. Res. Lett.*, *20*, 1711–1714.

Angelopoulos, V., C. Kennel, F. Coroniti, R. Pellat, M. Kivelson, R. Walker, C. Russell, W. Baumjohann, W. Feldman, and J. Gosling (1994), Statistical characteristics of bursty bulk flow events, *J. Geophys. Res.*, *99*, 21,257–21,280.

Auster, H. U., et al. (2008), The THEMIS Fluxgate Magnetometer, *Space Sci. Rev.*, *141*(1–4), 235–264.

Baker, D. N., T. I. Pulkkinen, V. Angelopoulos, W. Baumjohann, and R. L. McPherron (1996), Neutral line model of substorms: Past results and present view, *J. Geophys. Res.*, *101*, 12,975–13,010.

Balogh, A., et al. (2001), The Cluster Magnetic Field Investigation: Overview of in-flight performance and initial results, *Ann. Geophys.*, *19*(10), 1207–1217.

Baumjohann, W., G. Paschmann, and C. Cattell (1989), Average plasma properties in the central plasma sheet, *J. Geophys. Res.*, *94*, 6597–6606.

Baumjohann, W., G. Paschmann, and H. Lühr (1990), Characteristics of high-speed ion flows in the plasma sheet, *J. Geophys. Res.*, *95*, 3801–3809.

Borovsky, J. E., R. J. Nemzek, and R. D. Belian (1993), The occurrence rate of magnetospheric-substorm onsets: Random and periodic substorms, *J. Geophys. Res.*, *98*, 3807–3813.

Chua, D., G. Parks, M. Brittnacher, G. Germany, and J. Spann (2004), Auroral substorm timescales: IMF and seasonal variations, *J. Geophys. Res.*, *109*, A03207, doi:10.1029/2003JA009951.

Davis, T. N., and M. Sugiura (1966), Auroral electrojet activity index AE and its universal time variations, *J. Geophys. Res.*, *71*, 785–801.

Dungey, J. W. (1961), Interplanetary magnetic field and the auroral zones, *Phys. Rev. Lett.*, *6*, 47–48.

Frey, H. U. (2010), Comment on "Substorm triggering by new plasma intrusion: THEMIS all-sky imager observations" by Y. Nishimura et al., *J. Geophys. Res.*, *115*, A12232, doi:10.1029/2010JA016113.

Frey, H., and S. Mende (2006), Substorm onsets as observed by IMAGE-FUV, paper presented at 8th International Conference on Substorms, Can. Space Agency, Banff, Alberta.

Frey, H. U., S. B. Mende, V. Angelopoulos, and E. F. Donovan (2004), Substorm onset observations by IMAGE-FUV, *J. Geophys. Res.*, *109*, A10304, doi:10.1029/2004JA010607.

Henderson, M. G., G. D. Reeves, and J. S. Murphree (1998), Are north-south aligned auroral structures an ionospheric manifestation of bursty bulk flows?, *Geophys. Res. Lett.*, *25*, 3737–3740.

Hoffman, R. A., J. W. Gjerloev, L. A. Frank, and J. W. Sigwarth (2010), Are there optical differences between storm-time substorms and isolated substorms?, *Ann. Geophys.*, *28*(5), 1183–1198.

Jayachandran, P. T., and J. W. MacDougall (2007), Substorm time scales from polar cap convection measurements, *Earth Planets Space*, *59*(8), e29–e32.

Juusola, L., N. Østgaard, and E. Tanskanen (2011), Statistics of plasma sheet convection, *J. Geophys. Res.*, *116*, A08201, doi:10.1029/2011JA016479.

Kokubun, S., T. Yamamoto, M. H. Acuña, K. Hayashi, K. Shiokawa, and H. Kawano (1994), The GEOTAIL magnetic field experiment, *J. Geomagn. Geoelectr.*, *46*(1), 7–21.

Koskinen, H. E. J., R. E. Lopez, R. J. Pellinen, T. I. Pulkkinen, D. N. Baker, and T. Bösinger (1993), Pseudobreakup and substorm growth phase in the ionosphere and magnetosphere, *J. Geophys. Res.*, *98*, 5801–5813.

Kullen, A., and T. Karlsson (2004), On the relation between solar wind, pseudobreakups, and substorms, *J. Geophys. Res.*, *109*, A12218, doi:10.1029/2004JA010488.

Lui, A. T. Y., et al. (2008), Determination of the substorm initiation region from a major conjunction interval of THEMIS satellites, *J. Geophys. Res.*, *113*, A00C04, doi:10.1029/2008JA013424.

McFadden, J. P., C. W. Carlson, D. Larson, M. Ludlam, R. Abiad, B. Elliott, P. Turin, M. Marckwordt, and V. Angelopoulos (2008a), The THEMIS ESA plasma instrument and in-flight calibration, *Space Sci. Rev.*, *141*(1–4), 277–302.

McFadden, J. P., C. W. Carlson, D. Larson, J. Bonnell, F. Mozer, V. Angelopoulos, K.-H. Glassmeier, and U. Auster (2008b), THEMIS ESA first science results and performance issues, *Space Sci. Rev.*, *141*(1–4), 477–508.

McPherron, R. L. (1970), Growth phase of magnetospheric substorms, *J. Geophys. Res.*, *75*, 5592–5599.

McPherron, R. L. (1979), Magnetospheric substorms, *Rev. Geophys.*, *17*, 657–681, doi:10.1029/RG017i004p00657.

McPherron, R. L., C. T. Russell, and M. P. Aubry (1973), 9. Phenomenological model for substorms, *J. Geophys. Res.*, *78*, 3131–3149.

Milan, S. E., G. Provan, and B. Hubert (2007), Magnetic flux transport in the Dungey cycle: A survey of dayside and nightside reconnection rates, *J. Geophys. Res.*, *112*, A01209, doi:10.1029/2006JA011642.

Miyashita, Y., et al. (2009), A state-of-the-art picture of substorm-associated evolution of the near-Earth magnetotail obtained from superposed epoch analysis, *J. Geophys. Res.*, *114*, A01211, doi:10.1029/2008JA013225.

Mukai, T., S. Machida, Y. Saito, M. Hirahara, T. Terasawa, N. Kaya, T. Obara, M. Ejiri, and A. Nishida (1994), The low energy particle (LEP) experiment onboard the GEOTAIL satellite : GEOTAIL instruments and initial results. II, *J. Geomagn. Geoelectr.*, *46*(8), 669–692.

Nakamura, R., W. Baumjohann, M. Brittnacher, V. A. Sergeev, M. Kubyshkina, T. Mukai, and K. Liou (2001a), Flow bursts and auroral activations: Onset timing and foot point location, *J. Geophys. Res.*, *106*, 10,777–10,789.

Nakamura, R., W. Baumjohann, R. Schödel, M. Brittnacher, V. A. Sergeev, M. Kubyshkina, T. Mukai, and K. Liou (2001b), Earthward flow bursts, auroral streamers, and small expansions, *J. Geophys. Res.*, *106*, 10,791–10,802.

Nishimura, Y., S. Z. L. Lyons, V. Angelopoulos, and S. Mende (2010a), Substorm triggering by new plasma intrusion: THEMIS all-sky imager observations, *J. Geophys. Res.*, *115*, A07222, doi:10.1029/2009JA015166.

Nishimura, Y., L. R. Lyons, S. Zou, V. Angelopoulos, and S. B. Mende (2010b), Reply to comment by Harald U. Frey on "Substorm triggering by new plasma intrusion: THEMIS all-sky imager observations," *J. Geophys. Res.*, *115*, A12233, doi:10.1029/2010JA016182.

Ohtani, S., H. J. Singer, and T. Mukai (2006), Effects of the fast plasma sheet flow on the geosynchronous magnetic configuration: Geotail and GOES coordinated study, *J. Geophys. Res.*, *111*, A01204, doi:10.1029/2005JA011383.

Rème, H., et al. (2001), First multispacecraft ion measurements in and near the Earth's magnetosphere with the identical Cluster ion spectrometry (CIS) experiment, *Ann. Geophys.*, *19*(10), 1303–1354.

Sergeev, V. A., R. J. Pellinen, and T. I. Pulkkinen (1996), Steady magnetospheric convection: A review of recent results, *Space Sci. Rev.*, *75*, 551–604.

Shiokawa, K., W. Baumjohann, and G. Haerendel (1997), Braking of high-speed flows in the near-Earth tail, *Geophys. Res. Lett.*, *24*, 1179–1182.

Shue, J.-H., J. K. Chao, H. C. Fu, C. T. Russell, P. Song, K. K. Khurana, and H. J. Singer (1997), A new functional form to study the solar wind control of the magnetopause size and shape, *J. Geophys. Res.*, *102*, 9497–9511.

Tanskanen, E. I. (2009), A comprehensive high-throughput analysis of substorms observed by IMAGE magnetometer network: Years 1993–2003 examined, *J. Geophys. Res.*, *114*, A05204, doi:10.1029/2008JA013682.

L. Juusola, N. Partamies, K. Snekvik, and E. Tanskanen, Finnish Meteorological Institute, PO Box 503, FIN-00101 Helsinki, Finland. (liisa.juusola@fmi.fi; noora.partamies@fmi.fi; kristian.snekvik@fmi.fi; eija.tanskanen@fmi.fi)

N. Østgaard, Department of Physics and Technology, University of Bergen, Postboks 7803, NO-5020 Bergen, Norway. (nikolai.ostgaard@ift.uib.no)